International Journal of Industrial Engineering, 2018;2(5):108-118.
ISSN: 2456-8449.
http://ijie.gjpublications.com

Research Article

Performance of Pt–Ru–Mo Ternary Catalysts for Borohydride Electro-Oxidation in Membraneless Fuel Cell

M. Elumalai[1,2,*], A. Rajasekaran[2], B. Chinnaraja[3]

[1]Department of Chemistry, Presidency college (Autonomous), Chennai – 600 005. India.
[2]Department of Mathematics, Dhanalakshmi Srinivasan College of Engineering and Technology, Chennai. India.
[3]Department of Public Administration, University of Madras, Chennai – 600 005. India.

*Corresponding author's e-mail: mrelumalaimscphd@gmail.com

Abstract

Graphene supported Pt–Ru–Mo trimetallic electrocatalysts are prepared by the thermal decomposition of a polymeric precursor method, and used as the anode electrocatalysts for membraneless borohydride fuel cell (MLBFC). The physical and electrochemical properties of the as-prepared electrocatalysts are investigated by X-ray diffraction (XRD) analysis, transmission electron microscopy (TEM), cyclic voltammetry (CV), chronoamperometry (CA) and fuel cell test. XRD results show that the diffraction peaks in Pt–Ru–Mo/G catalysts shift slightly to higher 2θ values compared with that of Pt/G catalyst, suggesting the formation of Pt–Ru–Mo alloying. TEM results show that the morphologies of Pt–Ru–Mo trimetallic catalysts are uniformly spherical with the particle size of about 4.5 nm on the graphene surface. Besides, it has been found that the Pt–Ru–Mo/G (1:1:1) catalysts have much higher catalytic activity for the oxidation of sodium borohydride than Pt/G catalyst. The membraneless borohydride fuel cell with Pt–Ru–Mo/G (1:1:1) anode catalyst and Pt/G cathode catalyst obtains the maximum power density as high as 28.84 mW cm^{-2} at room temperature.

Keywords: Electrocatalysts; Electrochemical properties; Membraneles fuel cell; Chronoamperometry.

Introduction

Syntheses of nanaoparticles with controlled size and composition are great interest because nanoparticles possess unique physical and chemical properties [1]. Considerable effort has been devoted to develop electrocatalyst of the nanoscale metallic alloy for the sodium borohydride based fuel cells. The anode electrocatalyst is the key component in advancing the application of membraneless borohydride fuel cell (MLBFC). In the past few years, various materials have been studied as the anode electrocatalyst for the oxidation of BH_4^-, such as noble metals Pt, Os, Pd, Ag, transition metals Ni, Zn, and hydrogen storage alloys [2, 3]. To date, Pt is the most widely used catalyst material in fuel cells, but its high cost hinders a large-scale application in the fuel cell technologies. One promising way to lower the Pt catalyst costs is to alloy Pt with transition metals. Moreover, the Pt-based catalysts which alloyed with various transition metals have been claimed to be more active than pure Pt, and some of these catalysts have been reported to be two-fold more active [4]. Teogu et al. and co-workers studied the borohydride electro-oxidation on Pt, Pt–Ni and Pt–Co bimetallic electrodes, and found that the bimetallic Pt–Ni and Pt–Co catalysts exhibit a more negative open circuit potential and higher oxidation currents at low over potentials than Pt [5].

Sodium borohydride intermediate (BH_3OH^-) automatically-formed by sodium borohydride dehydrogenation are strongly adsorbed at the catalyst surface, thereby blocking the electrocatalytic active Pt sites. At fuel cell relevant-temperatures of about 80ºC, active platinum sites can only be freed from adsorbed BH_3OH^- by oxidative removal via oxygen-containing species nearby (water activation). However, pronounced water activation, providing these species near the blocked Pt atoms, take place at bulk Pt electrodes not below 700mV vs RHE. For this reason, binary and ternary catalyst formulations were developed,

Received: 08.05.2018; Received after Revision: 17.05.2018; Accepted: 18.05.2018; Published: 31.05.2018

which facilitate the formation of surface oxides at lower potentials. Thereby, the anodic overpotential is reduced, and increased power densities of the fuel cell can be achieved. Among the binary catalysts, the Pt–Ru/C binary metallic catalyst has been accepted as the best electrocatalyst for sodium borohydride oxidation in direct borohydride fuel cells [6]. However, the efficiency of direct borohydride fuel cells operating on Pt–Ru alloy catalysts is still insufficient for practical application. Many investigations have been made to improve the performance of the Pt–Ru/ binary catalyst with the incorporation of a third metal, such as Pt–Ru–Os/C, Pt–Ru–Sn/C, Pt–Ru–W/C and Pt–Ru–Mo/C [7-9]. The Pt–Ru/C electrocatalyst performance also depends greatly on preparation procedure and Pt:Ru atomic ratios. Many researchers studied that Ni can modify the behavior of the Pt–Ru/C electrocatalyst and act as an assistant component [10]. Therefore, the addition of Mo to Pt–Ru binary catalyst in the MLBFC would thus decrease the rate of borohydride hydrolysis reaction.

At the moment, a graphene-supported Pt–Ru–Mo (1:1:1) system is supposed to be the most active catalyst for MLBFC applications using sodium borohydride as a fuel. Nevertheless, numerous investigations on other binary and ternary systems have been reported recently, and the search for improved catalyst formulations is still going on.

Materials and methods

Materials

The metal precursors used for the preparation of electrocatalysts were $H_2PtCl_6.6H_2O$ (from Merck), $RuCl_3.3H_2O$ (from Sigma Aldrich), and $MoCl_2.2H_2O$ (from Sigma Aldrich). Graphene (purity of 97%, from Graphene Supermarket Supply) was used as support for the catalysts. Graphite plates (3-cm long and 0.1-cm wide from E-TEK) were used as substrates for the catalyst to prepare the electrodes. Polytetrafluoroethylene (PTFE) (6%; Aldrich) dispersion was used to prepare the catalyst slurry. Ascorbic acid (AA) (from Merck) was used as the reducing agent. Ethylene glycol (EG) (from Merck) and Isopropyl alcohol (from Merck) was used as a solvent. Sodium Borohydride (from Merck) + Sodium hydroxide (from Merck) and sodium perborate (from Riedel) + H_2SO_4 (from Merck) solution was used as the fuel and an oxidant respectively. All the chemicals were of analytical grade. Pt/G (40-wt%, from E-TEK) was used as the cathode catalyst.

Preparation of the graphene supported Pt–Ru–Mo catalysts

Graphene supported ternary Pt–Ru–Mo catalysts were prepared by the thermal decomposition of a polymeric precursor. The Pt, Ru and Mo polymeric precursors were separately prepared, mixing ascorbic acid (AA) in ethylene glycol (EG) at 60-65ºC. The metal precursor ($H_2PtCl_6.6H_2O$, $RuCl_3.3H_2O$ and $MoCl_2.2H_2O$–1M solution dissolved in isopropanol) were then added, so that an AA:EG:M 1:4:0.25 molar ratio (M = Pt, Ru and Mo) would be achieved. After total dissolution of the precursor salt, the temperature was raised to 90 ºC, and the mixture was kept under vigorous stirring for 2-3 h. Graphene, which had been previously treated for 4 h at 400 ºC under nitrogen atmosphere, was added to the precursor mixture, to obtain a catalyst loading of 40 wt.%. This mixture was finally dispersed in 2mL ethanol by ultrasonication for 10 min. Thermal treatments were carried out in a tubular oven under nitrogen atmosphere. The temperature was firstly increased to 250 ºC at a rate of 1 ºC/min and it was kept there for 1 h. Subsequently, the temperature was increased to 400 ºC at a rate of 30 ºC/min and kept there for 2 h. Finally after being cooled down to room temperature, the electrocatalysts were again kept in an oven under air atmosphere at 400 ºC for 1-2 h, to eliminate the excess carbon. For comparison, the monometallic Pt/G, bimetallic Pt–Ru/G and Pt–Mo/G catalysts were synthesized under the same conditions. The electrocatalytic mixtures and the atomic ratios were Pt/G (100), Pt–Mo/G (50:50), Pt–Ru/G (50:50) and Pt–Ru–Mo/G (1:1:1). The nominal loading of metals in the electrocatalysts was 40 wt.% and the remaining was 60 wt.% graphene.

Physicochemical characterization

The particle size distribution and mean particle size were also evaluated using TEM. The crystal structure of the synthesized electrocatalysts was characterized by powder X-ray diffraction (XRD) using a Rigaku multiflex diffractometer (model RU-200 B) with Cu–$K_{\alpha l}$ radiation source ($\lambda_{K\alpha l}$ = 1.5406 Å) operating at room temperature. The tube current was 40 mA

with a tube voltage of 40 kV. The 2θ angular regions between 20º and 90º were recorded at a scan rate 5º min^{-1} the mean particle size analyzed from TEM is verified by determining the crystallite size from XRD pattern using "Scherer" formula. Pt (2 2 0) diffraction peak was selected to calculate crystallite size and lattice parameter of platinum. According to Scherrer's eq. (1) [11].

$$d = \frac{0.9\lambda_{K\alpha 1}}{\beta_{2\theta} \cos \theta_{max}} \quad (1)$$

Where D is the average crystallite size, θ_{max} is the angle at the position of the peak maximum, $\beta_{2\theta}$ is the half width of the peak (in radians), 0.9 is the shape factor for spherical crystallite and $\lambda_{K\alpha l}$ is the wavelength of X-rays used. The lattice parameters of the catalysts were estimated according to eq. (2) [12].

$$a = \frac{\sqrt{2}\,\lambda_{K\alpha 1}}{\text{Sin}\,\theta_{max}} \quad (2)$$

Where a is the lattice parameter (nm) and all the other symbols have the same meanings as in equation 1. The atomic ratio of the catalysts was determined by an energy dispersive X-ray (EDX) analyzer, which was integrated with the TEM instrument.

Electrochemical measurement

Electrochemical studies of the electrocatalysts were carried out using the thin porous coating technique. All Electrochemical Measurements were performed on an electrochemical workstation (CH Instruments, Model CHI6650, USA) interfaced with a personal computer using the CHI software, at room temperature. A common three-electrode electrochemical cell using cyclic voltammetry (CV) and Chronoamperometry (CA) techniques was used for measurements. Catalysts coated glassy carbon electrode (GCE, 3 mm diameter and 0.071 cm^2 of electrode area, from CHI, USA) was used as the working electrode and platinum foil was used as the counter electrode. Ag/AgCl in saturated KCl was used as the reference electrode. The working electrode was prepared by applying catalyst ink made of 20 mg of electrocatalyst in a solution of 50 mL of water containing three drops of 6% PTFE suspension. The resulting mixture was treated in an ultrasound bath for 10 min to obtain a uniform dispersion. The catalyst slurry was then drop-cast on to a glassy carbon electrode and allowed to dry at 100˚C for 30 min. for assessing the electrocatalytic activity of the working electrode; cyclic voltammetry was obtained in 0.15 M sodium borohydride and 3 M NaOH solution with a scan rate of 20 mV S^{-1}. For the durability test, the chronoamperometric experiments were carried out at a potential step of –1.2 to –0.2 V for 600s in the same electrolyte. Before each measurement, the solution was purged with high-purity nitrogen gas for at least 30 min to ensure oxygen-free measurements.

Results and discussion

Physicochemical characterization of the Pt–Ru–Mo/G catalyst

XRD Analysis

XRD patterns reveal the bulk structure of the catalyst and its support. Fig. 1 shows the XRD patterns of the Pt/G (100), Pt–Mo/G (50:50), Pt–Ru/G (50:50) and Pt–Ru–Mo/G (1:1:1) catalysts. It can be seen that the first peak located at a 2θ value of about 25º in the XRD pattern is referred to graphene support.

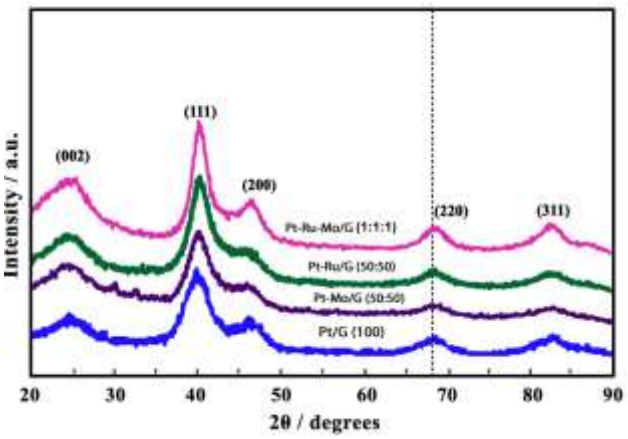

Fig. 1. X-Ray diffraction patterns of Pt/G (100), Pt–Mo/G (50:50), Pt–Ru/G (50:50)), and Pt–Ru–Mo/G (1:1:1) catalysts

The other four peaks located are characteristic of face centered cubic (fcc) crystalline Pt (Joint Committee on Powder Diffraction data JCPDS-ICDD, Card No. 04-802), corresponding to the planes (1 1 1), (2 0 0), (2 2 0) and (3 1 1) at 2θ values of about 40º, 47º, 68º and 82º, respectively, indicating that the alloy catalysts have principally single-phase disordered structure (i.e. solid solutions). Comparing with the reflections of pure Pt, the diffraction peaks for the Pt–Mo, Pt–Ru and Pt–Ru–Mo catalysts are shifted slightly to a higher

2θ values. The slight shift of the diffraction peaks reveal the formation of an alloy involving the incorporation of Ru and Mo atoms into the fcc structure of Pt. It is important to note that no diffraction peaks, indicating the presence of either pure Ru and Mo or Ru-rich hexagonal close packed (hcp) phase, and Mo oxide, appear.

The lattice parameters of Pt–Mo/G, Pt–Ru/G and Pt–Ru–Mo/G catalysts, which reflect the formation of a solid solution and be calculated by using the Pt (2 2 0) crystal faces, are given in Table 1. The lattice parameters obtained for the Pt–Mo/G, Pt–Ru/G, and Pt–Ru–Mo/G catalysts are smaller than those for Pt/G. In fact, the decrease in lattice parameters of the alloy catalysts reflects the progressive increase in the incorporation of Ru and Mo into the alloy state. Among four catalysts, the lattice parameter for Pt–Ru–Mo/G is the smallest, while that for Pt/G is the biggest. The average particle size *d* may be estimated from full width at half-maximum (FWHM) of Pt (2 2 0) according to Debye–Scherrer formula [13].

TEM Measurement

The TEM images Pt/G (100), Pt–Mo/G (50:50) and Pt–Ru–Mo/G (1:1:1) catalysts are shown in Fig.2 a-c, together with the obtained averaged value of the particle diameter distribution histograms.

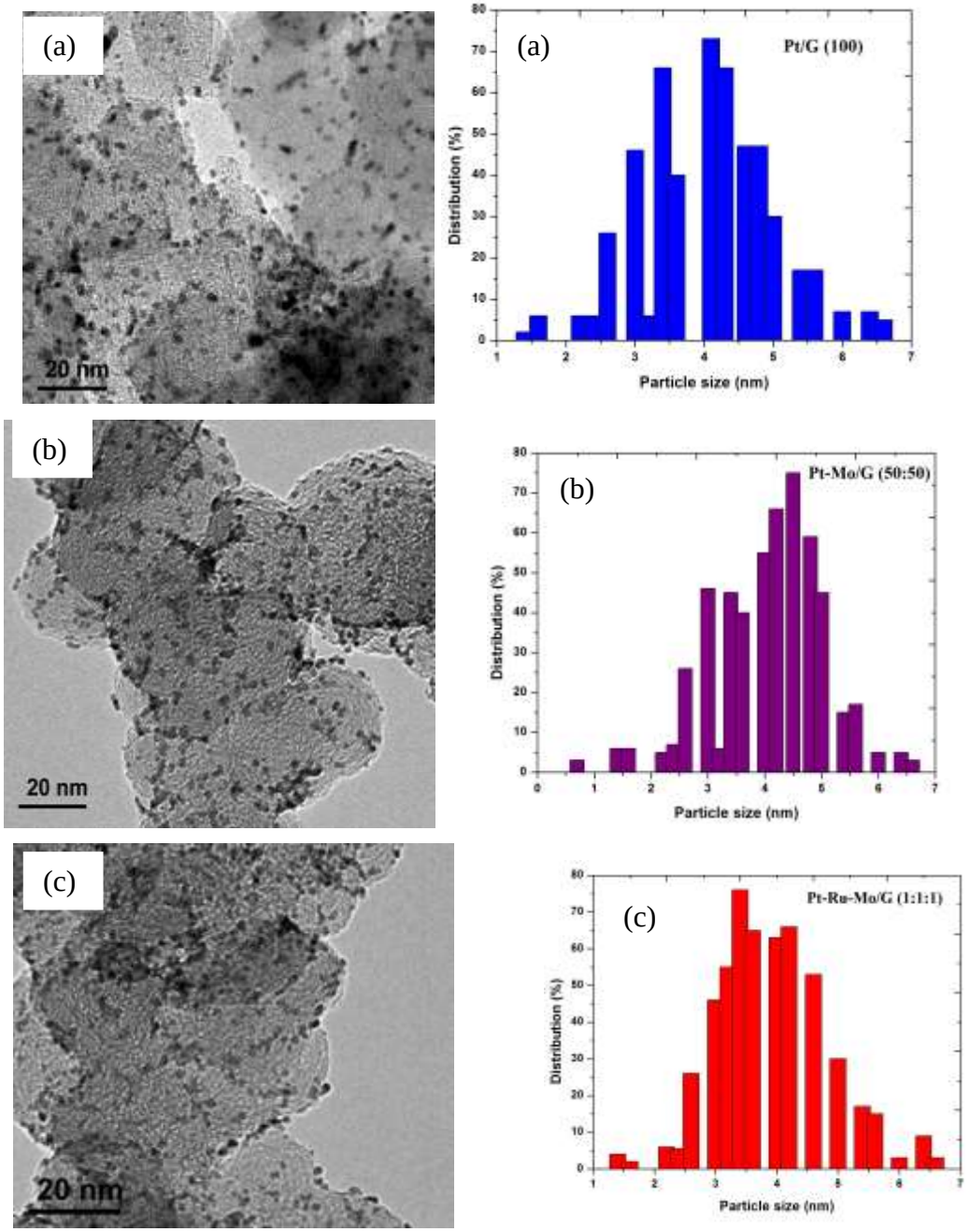

Fig. 2. TEM image and particle size histograms of (a) Pt/G, (b) Pt–Mo/G, (c) Pt–Ru–Mo/G catalysts

The micrographs of electrocatalysts show that all catalysts have a good dispersion on graphene with a size in the same range and follow a log-normal size distribution [14-18]. From the particle distribution of 1 to 7 nm, the average particle size for Pt–Mo/G (50:50), Pt–Ru/G (50:50) and Pt–Ru–Mo/G (1:1:1) catalysts were between 4 and 5 nm. In comparison to Pt–Mo/G (50:50), Pt–Ru/G (50:50) the mean particle size of Pt–Ru–Mo/G (1:1:1) was smaller. The variation of the mean particle size for the catalysts are quite similar in both cases (TEM and XRD), indicating a good particle dispersion without the formation of large particle aggregates (see Table 1).

EDX Spectrum

The EDX analyses of all the Pt–Mo/G (50:50), Pt–Ru/G (50:50) and Pt–Ru–Mo/G (1:1:1) catalysts are shown in Fig. 3. This image indicates the presence of Pt, Ru and carbon; Pt, Mo and carbon; and both the combination of Pt, Ru, Mo, and carbon, respectively. The EDX results are shown in Table 2. The catalysts prepared had the desired elements with some variation in composition. The EDX results of the binary Pt–Mo/G (50:50), Pt–Ru/G (50:50) and the ternary Pt–Ru–Mo/G (1:1:1) catalysts are very close to the nominal values, which indicate that the metals were loaded onto the graphene support without obvious loss.

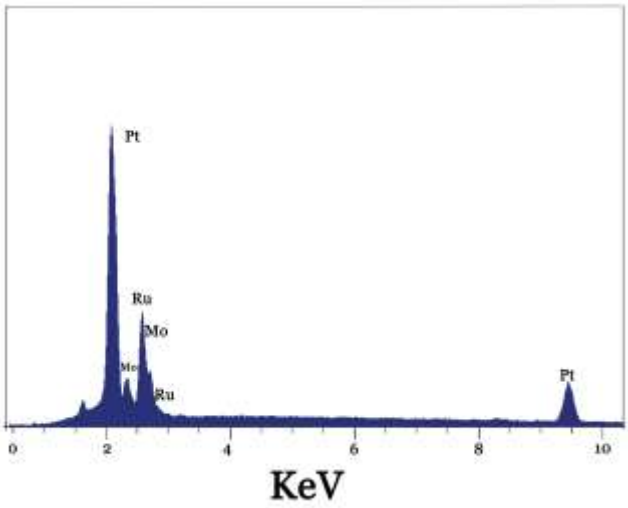

Fig. 3. EDX spectra of Pt–Ru–Mo/G (1:1:1) catalysts

Table 1. The EDX composition, lattice parameters and the particle size obtained for different atomic ratios of electrocatalysts.

Electrocatalysts	Nominal atomic ratio			EDX atomic ratio			lattice parameters (nm)	Crystallite size (nm)	Particle size from TEM (nm)
	Pt	Ru	Ni	Pt	Ru	Ni			
Pt/G	100	–	–	99	–	–	0.3915	4.5	4.1
Pt–Mo/G	50	–	50	51	–	49	0.3902	4.8	4.5
Pt–Ru/G	50	50	–	52	48	–	0.3888	4.6	4.3
Pt–Ru–Mo/G	34	33	33	36	32	32	0.3897	3.7	3.4

Electrochemical characterization of the Pt–Ru–Mo/G catalyst

CO stripping voltammetry

To investigate the catalytic of synthesized electrocatalysts supported on graphene for BOR and the performance of MLBFC, CO_{ads} stripping voltammograms were conducted in 0.5 M H_2SO_4 at room temperature. Fig.4 shows the CO_{ads} stripping voltammograms of Pt–Ru–Mo/G Pt–Ru/G, Pt–Mo/G, and Pt/G electrocatalysts at a CO adsorption potential of 0.07 V and a sweep rate of 50 mV s^{-1} between 0.05 V and 0.9 V versus Ag/AgCl. These conditions allowed elimination of all adsorbed CO during the first cycle, and the current in second cycle coincided with the baseline in the case of pure supporting electrolyte. The CO_{ads} oxidation peaks of the graphene substrate were observed at 0.35, 0.25, and 0.2 V vs. Ag/AgCl, for Pt/G, Pt–M/G (M = Mo and Ru) and Pt–Ru–Mo/G electrocatalysts, respectively. For the Pt–Ru–Mo/G electrocatalysts, there was a cathodic shift of at least 150 mV because of CO oxidation, compared to Pt/G. The peak positions in the voltammograms of the bimetallic Pt–M/G (M = Mo and Ru) and trimetallic Pt–Ru–Mo/G electrocatalysts were similar, but the peaks of the bimetallic electrocatalysts were less symmetric than those of Pt–Ru–Mo/G. The higher symmetry of the oxidation peak in the voltammograms of Pt–Ru–Mo/G. The higher symmetry of the oxidation peak in the voltammograms of Pt–Ru–Mo/G suggested that effective, strong electronic interactions took place between the Pt–Ru–Mo nanoparticles and graphene support.

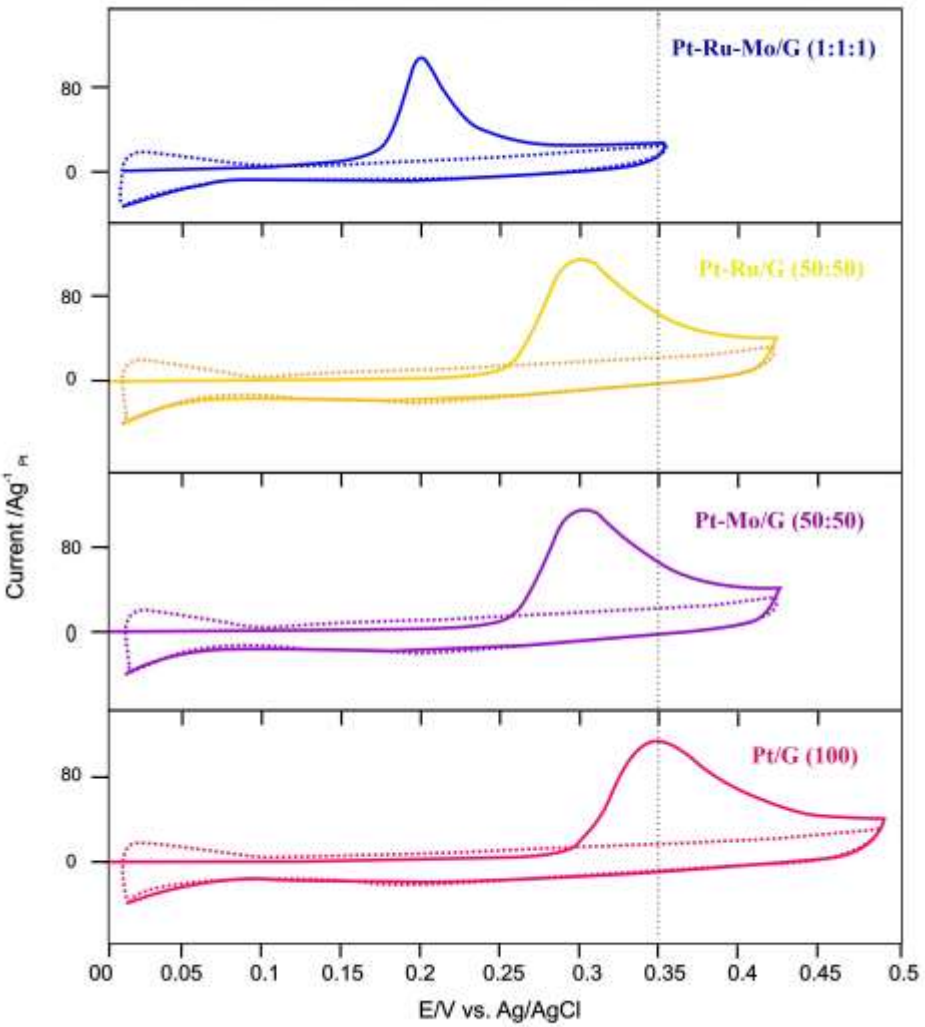

Fig. 4. CO stripping voltammograms of Pt–Ru–Mo/G (1:1:1), Pt–Ru/G (50:50), Pt–Mo/G (50:50) and Pt/G (100) electrocatalysts in 0.5 M H_2SO_4 at room temperature with a scan rate of 50 mV s^{-1}

Cyclic voltammetry

Fig. 5(a) shows representative cyclic voltammograms (CV) obtained for the Pt–Ru–Mo/G (1:1:1) electrocatalysts. The hydrogen adsorption/desorption region (0.0–0.4 V vs. Ag/AgCl) is poorly defined, and the current in the double layer region (0.4–0.8 V vs. Ag/AgCl) is higher compared with pure Pt-catalyst. This behavior is characteristic of supported graphene electrocatalysts containing transition metals. Taking the Pt/G (100) composition as reference, the binary Pt-catalyst incorporated with Ru or Ni has a voltammetric charge similar to that of the pure Pt catalyst. However, when both metals are simultaneously added to Pt to form ternary catalysts (Pt–Ru–Mo/G), a considerable increase in the voltammetric charge is observed.

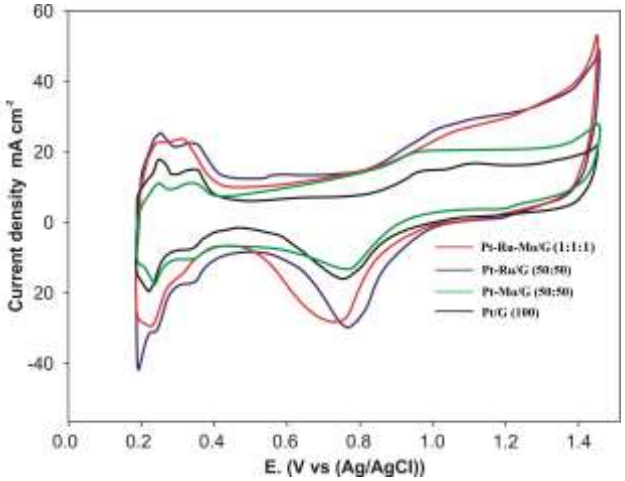

Fig. 5(a). Cyclic Voltammetry of Pt/G (100), Pt–Mo/G (50:50), Pt–Ru/G (50:50) and Pt–Ru–Mo/G (1:1:1) electrocatalysts in 0.5 M H_2SO_4 at room temperature with a scan rate of 50 mV s^{-1}

In order to investigate the electrocatalytic activity of the catalysts for sodium borohydride oxidation, the electrochemically active surface

area (S_{EAS}) was estimated using different procedures; namely CO adsorption ($S_{EAS/CO}$), hydrogen adsorption/desorption charge ($S_{EAS/H}$), and roughness of electrodes. The S_{EAS} values of the electrocatalysts were calculated by using eq. (3) and eq. (4) [15, 16].

$$S_{EAS/H}\,(m^2/g) = \frac{Q_H(\mu C/cm^2)}{210(\mu C/cm^2) \times 0.77 \text{ x } [Pt]} \quad (3)$$

$$S_{EAS/CO}\,(m^2/g) = \frac{Q_{CO}(\mu C/cm^2)}{420(\mu C/cm^2) \text{ x } [Pt]} \quad (4)$$

Where Q_H *and* Q_{CO} are the charges corresponding to desorption of hydrogen and CO on the Pt surface respectively, [Pt] (mg/cm^2) is the Pt loading on the electrode surface, 210 μC/real cm^2 and 420 μC/real cm^2 is the charge required to oxidize a monolayer of hydrogen and CO respectively on the Pt surface, 0.77 is the hydrogen monolayer coverage. The roughness of each electrode is calculated by dividing S_{EAS} obtained with the apparent surface area. Estimation of the electrode roughness and S_{EAS} values are shown in Table 2. Based on these values, the highest electrochemically active area is achieved for the ternary electrocatalysts.

Table 2. Comparison of hydrogen desorption charge and carbon monoxide desorption charge, and its electrochemical active surface area (S_{EAS}) and electrode roughness.

Catalyst	Q_H/ μC	Q_{CO}/ μC	Electrode real surface area (cm^2)	$S_{EAS/H}$ (m^{2}gPt^{-1})^a	$S_{EAS/CO}$ (m^{2}gPt^{-1})^a	Roughness
Pt/G (100)	437	1260	3.0	27	30	90.0
Pt–Mo/G (50:50)	226	735	1.8	28	35	63.0
Pt–Ru/G (50:50)	259	798	1.9	32	38	72.1
Pt–Ru–Mo/G (1:1:1)	209	657	1.6	38	46	73.6

Fig. 5b corresponds to representative cyclic voltammograms registered in the presence of sodium borohydride. All the current values were normalized by the geometric surface area of the electrode used. There were three oxidation peaks when sodium borohydride CV was carried out on the Pt/G catalyst (vs. Ag/AgCl), two during the forward scan and one during the reverse scan. The cyclic voltammetries (CV) recorded for Pt–Ru–Mo/G (1:1:1), Pt–Ru/G (50:50), Pt–Mo/G (50:50) and Pt/G (100) electrodes with 0.15 M $NaBH_4$ + 3 M NaOH solution at a scan rate of 20 mV s^{-1} in the potential range of –1.2 V to 0.6 V (vs. Ag/AgCl) are shown in Fig. 5b.

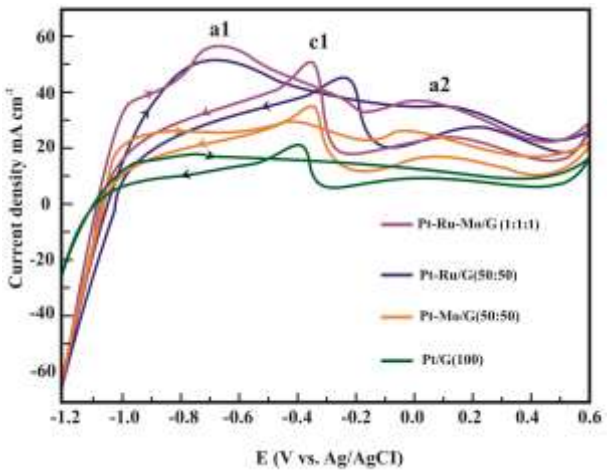

Fig. 5b. Cyclic Voltammetry of Pt/G (100), Pt–Mo/G (50:50), Pt–Ru/G (50:50) and Pt–Ru–Mo/G (1:1:1) electrocatalysts in 3 M NaOH and 0.15 M $NaBH_4$ at room temperature with a scan rate of 20 mV s^{-1}

Table 3. Cyclic Voltammetry results of Pt/G (100), Pt–Mo/G (50:50), Pt–Ru/G (50:50) and Pt–Ru–Mo/G (1:1:1) electrocatalysts at room temperature

Catalyst	Scan rate 20 mV s^{-1}	
	Positive peak potential (V vs. Ag/AgCl)	Peak current density (mA/cm^2)
Pt/G (100)	0.011	19.20
Pt–Mo/G (50:50)	0.025	26.61
Pt–Ru/G (50:50)	0.039	33.20
Pt–Ru–Mo/G (1:1:1)	0.045	35.30

According to the CV curves, the electrochemical performance of BH_4^- is fairly complex and characterized by a number of oxidation peaks. During the forward sweep, at a scan rate of 20 mV s^{-1}, a well-defined oxidation peaks rises at about –0.81 V (a1), followed by a anodic peak a1 and broad hump anodic peak (a2) which is observed. During the reverse sweep, a sharp anodic spike (c1) is noticed. The first anodic peak (a1) can be allocated to BH_4 hydrolysis followed by the electro-oxidation of H_2 (Eq. (4)), the second oxidation peak (a2) is attributed to the direct oxidation of BH^- in the absence of H_2 electro-oxidation, and the peak (c1) is due to the oxidation of absorbed intermediate oxidation product of BH_3OH^- (Eq. (5)) on the partially oxidized Pt surface.

$$BH_4^- + H_2O \rightarrow BH_3OH^- + H_2 \quad (4)$$

$$BH_3OH^- + 3OH^- \rightarrow BO_2^- + 3/2\ H_2 + 2H_2O + 3e^- \quad (5)$$

The onset potential for the oxidation of $NaBH_4$ in a positive scan was a significant factor for evaluating the catalyst's activity. The onset potentials for the oxidation of $NaBH_4$ on the Pt–Ru–Mo/G (1:1:1) (–1.069 V), electrocatalysts is slightly lower than that on the Pt–Ru/G (50:50) (–1.058 V), Pt–Mo/G (50:50) (–1.048 V) and Pt/G (100) (–1.025 V) catalysts. The CV curves illustrate the presence of a peak in the potential range of the positive sweep, and another peak in the negative sweep. The peak in the positive sweep is associated with the $NaBH_4$ oxidation, and the peak in the negative sweep is associated with the oxidation of BH_4 intermediate products from the partial oxidation of $NaBH_4$.

The peak current densities of peak a2 on Pt–Ru–Mo/G (1:1:1), Pt–Ru/G (50:50), Pt–Mo/G (50:50), and Pt/G (100) catalysts are 35.50, 33.20, 26.61and 19.20 mA cm^{-2}, respectively. Compared with Pt/G electrocatalyst, the peak current densities of peak a2 on Pt–Mo/G (50:50), Pt–Ru/G (50:50), Pt–Ru–Mo/G (1:1:1), electrodes are increased 38.5%, 69.3%, and 79.8%, respectively, indicating that the Pt–Ru–Mo/G (1:1:1) electrocatalysts can obviously improve the catalytic activity for BH_4^- oxidation. Table 3 summarizes the cyclic voltammagram results of Pt–Ru–Mo/G (1:1:1), Pt–Ru/G (50:50), Pt–Mo/G (50:50) and Pt/G (100) electrocatalysts including the a2 peak of positive peak potential and the peak current densities of BOR. The CV results show that pure Pt/G (100) catalysts do not perform as an appropriate anode for BOR, due to its hydrolysis of $NaBH_4$ that decreases the cell performance. However, the introduction of Ru and Mo promotes the electrocatalysts activity. CV for $NaBH_4$ oxidation reactions showed that the $NaBH_4$ hydrolysis was considerably inhibited by Pt–Ru–Mo/G (1:1:1) electrocatalyst, indicating the ability of Mo to promote direct oxidation of $NaBH_4$.

Chronoamperometry

Fig. 6 shows the current densities measured at a potential step of –1.2 to –0.2 V in 0.15 M $NaBH_4$ + 3 M NaOH at room temperature. The current decay with time in a parabolic style and reach an apparent steady state within 80s. It can be seen that the current density of sodium borohydride electro-oxidation on the Pt–Ru–Mo/G (1:1:1) catalyst is higher than that on the Pt–Ru/G (50:50), Pt–Mo/G (50:50), and Pt/G (100) catalyst at the same potentials. The activity change for sodium borohydride oxidation decreases in the order of Pt–Ru–Mo/G (1:1:1)> Pt–Ru/G (50:50)> Pt–Mo/G (50:50)> Pt/G (100), which is in fairly good agreement with our CV results for the durability test. Before each measurement, the solution was purged with high-purity nitrogen gas for at least 30 min to ensure oxygen-free measurements.

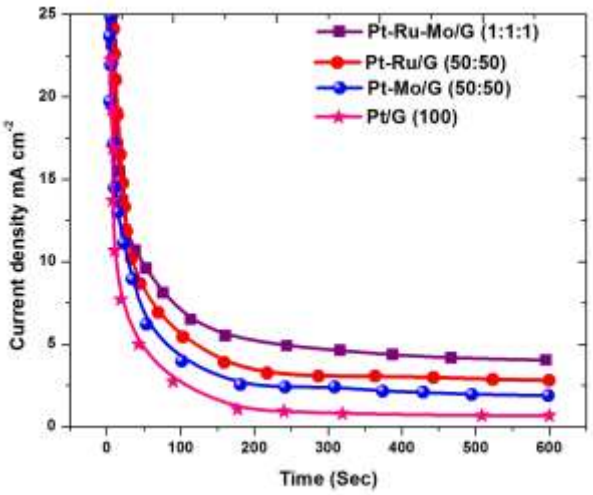

Fig. 6. CA of Pt/G (100), Pt–Mo/G (50:50), Pt–Ru/G (50:50) and Pt–Ru–Mo/G (1:1:1) electrocatalysts in 0.15 M $NaBH_4$ + 3 M NaOH at room temperature

Single cell performance

The microfluidic design of laminar flow-based membraneless fuel cells overcomes the fuel crossover and water management issues that plague membrane-based fuel cells (i.e., PEMFC, DMFC) and enables independent control of

stream characteristics (i.e., flow rate and composition). Here we focused on maximizing cell performance, in terms of power density, by tailoring various structural characteristics and catalytic activity of graphene supported ternary Pt–Ru–Mo catalysts. The Pt/G (100), Pt–Mo/G (50:50), Pt–Ru/G (50:50) and Pt–Ru–Mo/G (1:1:1) catalysts were evaluated as anode catalysts for borohydride electro-oxidation by single membraneless borohydride fuel cell (MLBFC), and the data are presented in Fig. 7.

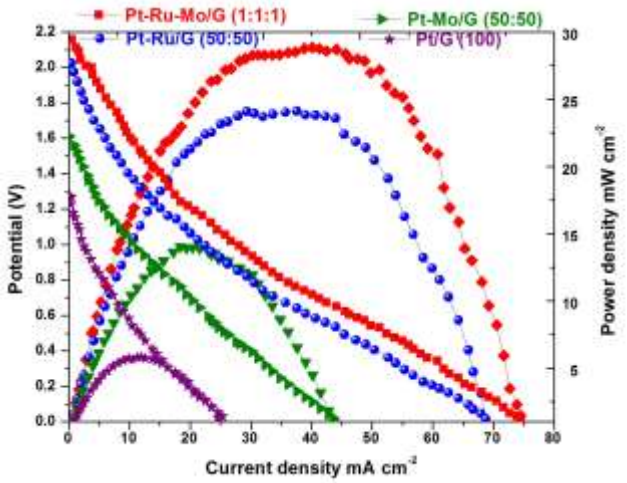

Fig. 7. Polarization and power density curves of different catalyst at 2 mg cm^{-2} catalyst loading on anode and cathode at room temperature. Anode feed: 0.15 M sodium borohydride in 3 M NaOH and Cathode feed: 0.15 M Sodium Perborate + 1.5 M H_2SO_4. Stream flow rates: 0.3 ml min^{-1}

When Pt/G (100) was used as the anode catalyst, the performance of single cell was poor. The open-circuit potential (OCP) was 1.27 V, which was mainly attributed to poor catalytic activity towards borohydride electro-oxidation. The maximum output power density for Pt/G (100) is 5.81 mW cm^{-2}. The results of MLBFC adapting to different catalysts are summarized in Table 4. When the current was normalized to the geometric area of single cell, it was observed that the cell performance of Pt–Ru–Mo/G (1:1:1) catalyst was better than other catalysts. In the low current discharging region, the power drawn from single cell was almost the same for all catalysts except Pt/G (100). However, as the voltage reach around 0.3 V Pt–Ru–Mo/G (1:1:1) started drawing more current in comparison to others.

The open-circuit potential for Pt–Mo/G (50:50) and Pt–Ru/G (50:50) catalysts was (1.61 V and 2.02 V respectively) lower than for Pt–Ru–Mo/G (1:1:1) (2.15 V). In addition, there was a rapid initial fall in cell voltage for all catalysts, which was due to the slow initial borohydride electro-oxidation reaction at the electrode surface. After an initial drop of 50 mV the change in slope of the polarization curve for Pt–Ru–Mo/G (1:1:1) decreased, and it started drawing more current. This is attributed to the more effective catalytic ability of Pt–Ru–Mo/G (1:1:1), once the borohydride electro-oxidation reaction being initiated. Based on peak power density drawn from single cell, Pt–Ru–Mo/G (1:1:1) is the best anode catalyst with peak power density value of 28.84 mW cm^{-2}. The results are similar to those of cyclic voltammetric and chronoamperometric measurements. Fig. 8 shows the peak current density of the Pt–Ru–Mo/G (1:1:1) electrocatalyst was higher than that of the Pt–Ru/G (50:50), Pt–Mo/G (50:50), and Pt/G (100) catalysts.

As discussed previously the addition of small quantities of Mo to Pt–Ru/G catalyst produced the superior performance of Pt–Ru–Mo/G electrocatalysts for borohydride electro-oxidation due to the promoting effect of Mo.

Table 4. Summary of performance of fuel cell tests using 2 mg cm^{-2} catalyst loading, (40 wt% catalysts on graphene)

Anode Catalysts	Open circuit Potential (V)	Maximum power density (mW cm^{-2})	Maximum Current density (mA cm^{-2})
Pt/G (100)	1.27	5.81	25.29
Pt–Mo/G (50:50)	1.61	14.01	43.64
Pt–Ru/G (50:50)	2.02	24.11	68.76
Pt–Ru–Mo/G (1:1:1)	2.15	28.84	74.50

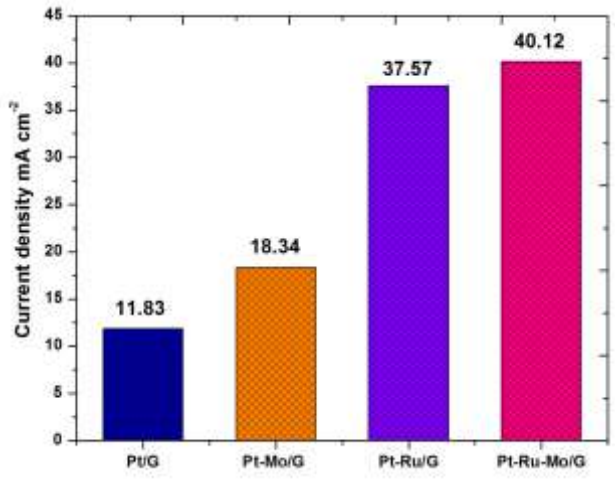

Fig. 8. Peak current density of Pt/G (100), Pt–Mo/G (50:50), Pt–Ru/G (50:50) and Pt–Ru–Mo/G (1:1:1) electrocatalysts at room temperature. Anode feed: 0.15 M sodium borohydride in 3 M NaOH and Cathode feed: 0.15 M Sodium Perborate + 1.5 M H_2SO_4. Stream flow rates: 0.3 ml min^{-1}

Conclusions

The graphene-supported Pt–Ru–Mo, Pt–Ru, Pt–Mo and Pt electrocatalysts with the physically-mixed and alloy structure were successfully prepared and analyzed with XRD, TEM and EDX measurements. A uniform dispersion of the metal nanoparticles on the graphene support with the intended compositions has been confirmed by EDX and TEM analysis. The TEM images indicated an average particle size of Pt–Ru–Mo/G (1:1:1) nanoparticle of 3-5 nm. EDX reveals that the Mo content is lower than the nominal value. In XRD analysis the diffraction peaks for the Pt–Mo, Pt–Ru and Pt–Ru–Mo catalysts are shifted slightly to a higher 2θ values. The slight shift of the diffraction peaks reveal the formation of an alloy involving the incorporation of Ru and Mo atoms into the fcc structure of Pt. Electrochemical tests CV, CA have been performed to compare the BOR activities of the catalysts. Among the various catalysts investigated, the Pt–Ru–Mo/G (1:1:1) catalyst exhibits the highest BOR activity, followed by the Pt–Ru/G (50:50), Pt–Mo/G (50:50) and Pt/G (100) catalysts. From the electrochemical data, it is seen that the incorporation of a small amount of Mo into Pt–Ru/G further enhances the BOR activity. The MLBFC employing Pt–Ru–Mo/G (1:1:1) as anode catalyst and Pt/G as cathode catalyst obtained the maximum power density is 28.84 mW cm^{-2} at room temperature. From the electrochemical tests and single cell test, the graphene-supported Pt–Ru–Mo (1:1:1) catalysts offer the potential to be considered as an alternative anode catalyst for MLBFCs. Further work is necessary to characterize the catalysts using different surface analysis techniques and to conduct test of these electrocatalysts in membraneless borohydride fuel cells

Conflicts of interest

Authors declare no conflict of interest.

References

[1] Elumalai M, Priya M, Kiruthika S, Muthukumaran B. Effect of Ni on graphene supported Pt–Ru binary catalyst for borohydride electro-oxidation. International Journal of Industrial Engineering. 2017;1(2):67-77.

[2] De Leon CP, Walsh FC, Pletcher D, Browning DJ, Lakeman JB. Direct borohydride fuel cells. J Power Sources. 2006;155(2):172-81.

[3] Wee JH, Which type of fuel cell is more competitive for portable application: direct methanol fuel cells or direct borohydride fuel cells?. J Power Sources. 2006;161(1):1-10 .

[4] Priya M, Elumalai M, Kiruthika S, Muthukumaran B. Influences of supporting materials for Pt-Ru binary catalyst in Ethanol fuel cell. International Journal of Modern Science and Technology. 2016;1(1):5-11.

[5] Mahendran S, Anbuselvan C. Kinetics and mechanism of oxidation of 5-(4‟-bromophenyl)-5-oxopentanoic acid by acid permanganate. International Journal of Modern Science and Technology. 2016; 3(1):106-10.

[6] Li ZP, Liu BH, Arai K, Asaba K, Suda S. Evaluation of alkaline borohydride solutions as the fuel for fuel cell. J Power Sources. 2004;126(2):28-33.

[7] Sung W, Choi JW. A membraneless microfuel cell using non-noble catalysts in alkaline solution. J Power Sources. 2007;172(1):198-208.

[8] Mousavi Shaegh SA, Nguyen NT, Chan SH. Air-breathing membraneless laminar flow-based fuel cell with flow-through anode, Int J Hydrogen Energy. 2011;37(4):3466-76.

[9] Flipsen SFJ. Power sources compared; The ultimate truth?, J Power Sources. 2006;162(2):927-34.
[10] Kjeang E, Djilali N, Sinton D. Microfluidic fuel cells; A review. J Power Sources. 2009;186(2):353-69.
[11] De Jong J, Lammertink RGH, Wessling M. Membraneless and microfluidic: A review. Lab on a Chip. 2006;6:1125-39.
[12] Santos DMF, Sequeira CAC. Sodium borohydride as a fuel for the future. Renew Sustain Energ Rev. 2011;15(8):3980-4016.
[13] Santos DMF, Sequreira CAC. On the electrosynthesis of sodium borohydride. Int J Hydrogen Energy. 2010;35:9851-61.
[14] Elumalai M, Priya M, Kiruthika S, Muthukumaran B. Effect of acid and alkaline media on membraneless fuel cell using sodium borohydride as a fuel. J Afinidad. 2015;72:572.
[15] Mitrovski SM, Nuzzo RG. A passive microfluidic hydrogen-air fuel cell with exceptional stability and high performance. Lab on a Chip. 2006;6(3): 353-61.
[16] Choban ER, Waszczuk P, Kenis PJA, Characterization of limiting factors in laminar flow-based membraneless microfuel cell. Electrochem Solid State Lett. 2005;8(7):A348-52.
[17] Cheng H, Scott K, Influence of operating conditions on direct borohydride fuel cell performance. J Power Sources. 2006;160(1):407-12.
[18] Kalaikathir SPR, Begila David S. Synthesis and characterization of nanostructured carbon-supported Pt electrocatalysts for membraneless methanol fuel cells. International Journal of Modern Science and Technology. 2016;1(6):199-212.

****

